Published in final edited form as:
Eur J Neurosci. 2011 December ; 34(11): 1724–1736. doi:10.1111/j.1460-9568.2011.07886.x.

Developmental regulation of G protein-gated inwardly-rectifying K^+ (GIRK/K_{IR}3) channel subunits in the brain

Laura Fernández-Alacid[1], **Masahiko Watanabe**[2], **Elek Molnár**[3], **Kevin Wickman**[4], and **Rafael Luján**[1]

[1]Departamento de Ciencias Médicas, Instituto de Investigación en Discapacidades Neurológicas (IDINE), Facultad de Medicina, Universidad de Castilla-La Mancha, Campus Biosanitario, C/ Almansa 14, 02006 Albacete, Spain

[2]Department of Anatomy, Hokkaido University School of Medicine, Sapporo, Japan

[3]MRC Centre for Synaptic Plasticity, School of Physiology and Pharmacology, University of Bristol, Medical Sciences Building, Bristol, UK

[4]Department of Pharmacology, University of Minnesota, Minneapolis, MN, USA

Abstract

G protein-gated inwardly-rectifying K^+ (GIRK/family 3 of inwardly-rectifying K^+) channels are coupled to neurotransmitter action and can play important roles in modulating neuronal excitability. We investigated the temporal and spatial expression of GIRK1, GIRK2 and GIRK3 subunits in the developing and adult rodent brain using biochemical, immunohistochemical and immunoelectron microscopic techniques. At all ages analysed, the overall distribution patterns of GIRK1-3 were very similar, with high expression levels in the neocortex, cerebellum, hippocampus and thalamus. Focusing on the hippocampus, histoblotting and immunohistochemistry showed that GIRK1-3 protein levels increased with age, and this was accompanied by a shift in the subcellular localization of the subunits. Early in development (postnatal day 5), GIRK subunits were predominantly localized to the endoplasmic reticulum in the pyramidal cells, but by postnatal day 60 they were mostly found along the plasma membrane. During development, GIRK1 and GIRK2 were found primarily at postsynaptic sites, whereas GIRK3 was predominantly detected at presynaptic sites. In addition, GIRK1 and GIRK2 expression on the spine plasma membrane showed identical proximal-to-distal gradients that differed from GIRK3 distribution. Furthermore, although GIRK1 was never found within the postsynaptic density (PSD), the level of GIRK2 in the PSD progressively increased and GIRK3 did not change in the PSD during development. Together, these findings shed new light on the developmental regulation and subcellular diversity of neuronal GIRK channels, and support the contention that distinct subpopulations of GIRK channels exert separable influences on neuronal excitability. The ability to selectively target specific subpopulations of GIRK channels may prove effective in the treatment of disorders of excitability.

Keywords

electron microscopy; family 3 of inwardly-rectifying K^+ channels; G protein-gated inwardly-rectifying K^+ channel; histoblot; immunohistochemistry

Correspondence: Dr Rafael Luján, as above. Rafael.Lujan@uclm.es.

Introduction

G protein-gated inwardly rectifying K^+ (GIRK/family 3 of inwardly-rectifying K^+) channels contribute to the regulation of membrane excitability in the brain, and play key roles in synaptic plasticity and behaviour (Lüscher *et al.*, 1997; Lüscher & Slesinger, 2010). GIRK channels constitute a critical effector of G protein-coupled receptors that use the Gi/o family of G proteins, thus mediating their slow inhibitory effects (Lüscher & Slesinger, 2010). A major G protein-coupled receptor activating GIRK channels is the metabotropic γ-aminobutyric acid type B ($GABA_B$) receptor (Lüscher *et al*., 1997). Macromolecular signalling complexes containing $GABA_B$ receptors and GIRK channels exist in the brain (Ciruela *et al*., 2010; David *et al.*, 2006; Fernández-Alacid *et al.*, 2009; Fowler *et al*., 2007), indicating that their spatial proximity is a critical mechanism to ensure their functional association.

Four different genes encode GIRK channel subunits in mammals (GIRK1–4), which combine to form functional homotetrameric or heterotetrameric channels (Krapivinsky *et al.*, 1995; Lesage *et al*., 1995). Three channel subunits (GIRK1–GIRK3) exhibit broad and partly overlapping distributions in the central nervous system, whereas GIRK4 expression is limited to a small number of neuron populations (Karschin *et al*., 1996; Perry *et al.*, 2008; Wickman *et al.*, 2000). The overlapping distribution of neuronal GIRK channels suggests the potential for considerable molecular diversity (Karschin *et al.*, 1996). In the brain, GIRK2 contributes to the formation of most GIRK channels (reviewed by Luján *et al*., 2009; Lüscher & Slesinger, 2010), determining their assembly and surface localization (Inanobe *et al*., 1999). The GIRK1 subunit assembles with GIRK2 (Koyrakh *et al*., 2005; Liao *et al*., 1996; Marker *et al*., 2004), and the similar electrophysiological profiles of neurons from $GIRK1^{-/-}$ and $GIRK2^{-/-}$ mice support this notion (Koyrakh *et al*., 2005; Marker *et al*., 2006). Recent evidence suggests that many GIRK channel subtypes exist in the brain in a cell type- and subcellular compartment-dependent manner (Aguado *et al*., 2008; Ciruela *et al.*, 2010; Fernández-Alacid *et al.*, 2009; Labouèbe *et al*., 2007; Perry *et al*., 2008). For instance, the GIRK3 subunit also seems to add to the repertoire of functional GIRK channels in the brain. In the cerebellum, ultrastructural data have shown that dendritic spines of Purkinje cells and dendrites of granule cells contain GIRK1, GIRK2 and GIRK3 (Ciruela *et al.*, 2010; Fernández-Alacid *et al.*, 2009). However, membrane fractionation analyses have indicated that GIRK2 and GIRK3 are present in distinct membrane microdomains in the hippocampus (Koyrakh *et al.*, 2005), suggesting that the relevance of the GIRK3 subunit in the formation of functional GIRK channels in the hippocampus is different to that in the cerebellum.

Information regarding the ontogeny and distribution of GIRK channel subunits is crucial to elucidate the contribution of the ion channels to developmental processes and hippocampal functions. Therefore, affinity-purified GIRK subunit-specific antibodies were used to understand how GIRK channel subunit expression develops during postnatal development and becomes organized along the surface of pyramidal cells using histoblotting and immunoelectron microscopy approaches, combined with quantitative analyses.

Materials and methods

Tissue preparation

The OF-1 mice and Wistar rats from the day of birth [postnatal day (P)0] to adulthood (P60) (obtained from the Animal House Facility of the School of Medicine of the University of Castilla-La Mancha) were used for histoblots, and light and electron microscopy immunohistochemical analyses. The animals were housed on a 12 h light/dark cycle, with food and water available *ad libitum*. The care and handling of the animals prior to and

during the experimental procedures followed Spanish and European Union regulations, and were approved by the Animal Care and Use Committee of the institution. For each developmental stage, the animals used were from different litters.

For histoblotting, animals were deeply anaesthetized by hypothermia (P0-P5) or by intraperitoneal injection of ketamine/xylazine 1 : 1 (0.1 mL/kg b.w.) and the brains were quickly frozen in liquid nitrogen. For immunohistochemistry, animals were anaesthetized and transcardially perfused with ice-cold fixative containing 4% paraformaldehyde and 15% (v/v) saturated picric acid (also containing 0.05% glutaraldehyde for electron microscopy) made up in 0.1 M phosphate buffer (pH 7.4). After perfusion, brains were removed and immersed in the same fixative for 2 h or overnight at 4 °C. Tissue blocks were washed thoroughly in 0.1 M phosphate buffer. Coronal 60-μm-thick sections were cut on a Vibratome (Leica V1000).

Antibodies

Rabbit anti-GIRK1 polyclonal, guinea pig anti-GIRK2 polyclonal and rabbit anti-GIRK3 polyclonal antibodies (Aguado *et al.*, 2008) were used in this study. The detailed characterization of the antibodies targeting GIRK channel subunits has been described elsewhere (Aguado *et al.*, 2008; Fernández-Alacid *et al.*, 2009).

Histoblotting

The regional distribution of GIRK channel subunits was analysed in rodent brains, using an *in-situ* blotting technique (histoblot) (Tönnes *et al.*, 1999). For this technique, the expression patterns for GIRK1 and GIRK2 were determined in mouse brains, whereas that for GIRK3 was determined in rat brains; a number of attempts to detect GIRK3 in mouse brains did not yield reliable labelling (Supporting Information Fig. S1). Briefly, horizontal cryostat sections (10 μm) from mouse or rat brain were apposed to nitrocellulose membranes moistened with 48 mM Tris-base, 39 mM glycine, 2% (w/v) sodium dodecyl sulphate and 20% (v/v) methanol for 15 min at room temperature (~20 °C). After blocking in 5% (w/v) non-fat dry milk in phosphate-buffered saline, nitrocellulose membranes were treated with DNase I (5 U/mL), washed and incubated in 2% (w/v) sodium dodecyl sulphate and 100 mM β-mercaptoethanol in 100 mM Tris–HCl (pH 7.0) for 60 min at 45 °C to remove adhering tissue residues. After extensive washing, the blots were reacted with affinity-purified anti-GIRK1, anti-GIRK2 and anti-GIRK3 antibodies (0.5 mg/mL) in blocking solution overnight at 4 °C. The bound primary antibodies were detected with alkaline phosphatase-conjugated anti-rabbit or anti-guinea pig IgG secondary antibodies (Tönnes *et al.*, 1999). A series of primary and secondary antibody dilutions and incubation times were used to optimize the experimental conditions for the linear sensitivity range of the alkaline phosphatase reactions. To compare the expression levels of each protein during development, all nitrocellulose membranes were processed in parallel, and the same incubation time for each reagent was used for all antibodies at all ages. Therefore, some regions that showed very low levels of expression may have been considered as negative. For this reason, we only performed quantitative analysis on the expression levels from P5. We only compared labelling intensities obtained with the same antibody.

To facilitate the identification of brain regions, structures and cell layers, adjacent cryostat sections were stained with cresyl violet at all developmental ages (Supporting Information Fig. S2). Digital images were acquired by scanning the nitrocellulose membranes using a desktop scanner (HP Scanjet 8300). Image analysis and processing were performed using the Adobe Photoshop software (Adobe Systems, San José, CA, USA) as described previously (Kopniczky *et al.*, 2005). The same incubation time for each reagent was used for all antibodies. All of the images were processed with the same equipment in the same way to

allow comparison of the intensity of grayscale images at different postnatal ages and in different brain regions on different days. The pixel density (arbitrary units) of immunoreactivity was measured using open circular cursors with a diameter of 0.10 mm. The cursors were placed in different brain regions identified based on the adjacent cresyl violet-stained sections (Kopnoczky *et al.*, 2005). We used background correction to eliminate potential differences in optical densities across different sections in different experiments. The average of eight background determinations carried out near the brain protein-containing areas of the immunostained nitrocellulose membranes was subtracted from the average pixel densities measured within brain regions. Following background corrections, the average pixel density for the whole region from one animal counted as one 'n'. Under these conditions, labelling performed on different days produced very consistent results. Data were analysed and plotted using the software Analysis (Soft Imaging Systems, Munster, Germany).

Immunohistochemistry for light microscopy

Sections were incubated in 10% (v/v) normal goat serum (NGS) diluted in 50 mm Tris buffer (pH 7.4) containing 0.9% (v/v) NaCl [Tris-buffered saline (TBS)], with 0.2% (v/v) Triton X-100 for 1 h. Sections were then incubated for 48 h in either anti-GIRK1, anti-GIRK2 or anti-GIRK3 at a final protein concentration of 1–2 μg/mL diluted in TBS containing 1% (v/v) NGS. After several washes in TBS, the sections were further incubated for 2 h in biotinylated goat anti-rabbit IgG or anti-guinea pig IgG (Vector Laboratories, Burlingame, CA, USA) diluted 1 : 100 in TBS containing 1% (v/v) NGS. They were then transferred into avidin–biotin–peroxidase complex (ABC kit; Vector Laboratories), diluted 1 : 100, for 2 h at room temperature. Bound peroxidase enzyme activity was revealed using 3,3′-diaminobenzidine tetrahydrochloride (0.05% in Tris buffer, pH 7.4) as the chromogen and 0.01% (v/v) H_2O_2 as the substrate. Finally, sections were air-dried and coverslipped prior to observation in a Nikkon photomicroscope (Nikkon, Eclipse 80i) equipped with differential interference contrast optics and a digital imaging camera.

Immunohistochemistry for electron microscopy

Immunohistochemical reactions for electron microscopy were carried out using the immunogold methods described previously (Luján *et al.*, 1996). Ultrastructural analyses were performed in a Jeol-1010 electron microscope.

Pre-embedding immunogold method—Briefly, free-floating sections were incubated in 10% (v/v) NGS diluted in TBS. Sections were then incubated in anti-GIRK1, anti-GIRK2 or anti-GIRK3 antibodies [3-5 μg/mL diluted in TBS containing 1% (v/v) NGS], followed by incubation in goat anti-rabbit or anti-guinea pig IgG coupled to 1.4 nm gold (Nanoprobes Inc., Stony Brook, NY, USA). Sections were postfixed in 1% (v/v) glutaraldehyde and washed in double-distilled water, followed by silver enhancement of the gold particles with an HQ Silver kit (Nanoprobes Inc.). Sections were then treated with osmium tetraoxide (1% in 0.1 M phosphate buffer), block-stained with uranyl acetate, dehydrated in graded series of ethanol and flat-embedded on glass slides in Durcupan (Fluka) resin. Regions of interest were cut at 70-90 nm on an ultramicrotome (Reichert Ultracut E, Leica, Austria) and collected on single slot pioloform-coated copper grids. Staining was performed on drops of 1% aqueous uranyl acetate followed by Reynolds's lead citrate.

Postembedding immunogold method—Briefly, ultrathin sections (80 nm thick) from Lowicryl-embedded blocks of hippocampus were collected on single slot pioloform-coated nickel grids and incubated on drops of a blocking solution consisting of 2% human serum albumin in 0.05 M TBS and 0.03% (v/v) Triton X-100. The grids were incubated with GIRK1, GIRK2 or GIRK3 antibodies [10 μg/mL in 0.05 M TBS and 0.03% (v/v) Triton

X-100 with 2% (w/v) human serum albumin] at 28 °C overnight. The grids were incubated on drops of goat anti-guinea pig IgG or goat anti-rabbit IgG conjugated to 10 nm colloidal gold particles (Nanoprobes) in 2% (w/v) human serum albumin and 0.5% (w/v) polyethylene glycol in 0.05 M TBS and 0.03% (v/v) Triton X-100. The grids were then washed in TBS and counterstained for electron microscopy with saturated aqueous uranyl acetate followed by lead citrate.

Quantification of GIRK channel subunits during development

To establish the relative abundance of GIRK channel subunits in CA1 pyramidal cells during development, quantification of immunolabelling was carried out in three different ways. (i) To determine the abundance of GIRK1, GIRK2 and GIRK3 immunoreactivity in different compartments of pyramidal cells during development, we used 60 μm coronal slices processed for pre-embedding immunogold immunohistochemistry. The procedure was similar to that used previously (Luján *et al.*, 1996; Luján & Shigemoto, 2006). Briefly, for each of three animals from different postnatal ages and adult, three samples of tissue were obtained for the preparation of embedding blocks (totalling nine blocks for each age). To minimize false negatives, ultrathin sections were cut close to the surface of each block. We estimated the quality of immunolabelling by always selecting areas with optimal gold labelling at approximately the same distance from the cutting surface. Randomly selected areas were then photographed from the selected ultrathin sections at a final magnification of 45 000×. Quantification of immunogold labelling was carried out in reference areas totalling approx. 2000 μm^2 for each age. Immunoparticles identified in each reference area and present along the plasma membrane and intracellular sites in dendrites, spines and axon terminals were counted. (ii) To establish the relative abundance of GIRK1, GIRK2 and GIRK3 immunoreactivity at synaptic sites during postnatal development, quantification of immunolabelling at excitatory synapses was performed in single sections in the distal part of the *stratum radiatum* from 80 nm ultrathin sections obtained from Lowicryl-embedded blocks. Only synapses made by axon terminals with CA1 pyramidal cell spines were evaluated for the number of gold particles per synapse (both labelled and unlabelled) or number of gold particles per labelled synapse; labelled synapses had one or more gold particles. Synapses were only included in the analysis if the synaptic cleft was visible. (iii) To establish the density of GIRK1, GIRK2 and GIRK3 at extrasynaptic sites in dendritic spines of CA1 pyramidal cells in the adult, quantification of immunolabeling was performed from 60 μm coronal slices processed for pre-embedding immunogold in three different layers: the proximal *stratum radiatum* (defined as the portion in the 100 μm away from the *stratum pyramidale*), distal *stratum radiatum* (defined as the portion in the 100 μm away from the border of the *stratum lacunosum–moleculare*) and *stratum lacunosum–moleculare*. For each of three animals from different postnatal ages and adult, three samples of tissue were obtained. Randomly selected areas were then photographed from the selected ultrathin sections at a final magnification of 45 000×. Quantification of immunogold labelling was carried out in reference areas totalling approx. 2000 μm^2 for each age. Immunoparticles identified in dendritic spines were counted and the surface area of each spine was measured. The data (density of GIRK subunits in spines in each CA1 layer) were expressed as the number of immunoparticles/μm^2. We calculated the non-specific labelling density in every reaction in the nuclei of pyramidal cells, a subcellular compartment that should not contain any GIRK. The immunoparticle density over the nuclei was 0.04 ± 0.01 immunoparticles/μm^2.

Controls

To test the method specificity in the procedures for histoblotting, as well as for both light and electron microscopy, antisera against GIRK1, GIRK2 and GIRK3 were tested on brain slices of mice lacking the corresponding channel subunit (Supporting Information Fig. S3)

(Aguado *et al.*, 2008; Fernández-Alacid *et al.*, 2009). Furthermore, the primary antibody was either omitted or replaced with 5% (v/v) normal serum of the species of the primary antibody. Under these conditions, no selective labelling was observed.

Statistical analysis

Statistical analyses were performed using Analysis (Soft Imaging Systems) and data are presented as mean ± SEM. For histoblotting and electron microscopic techniques, statistical differences during development between the brain regions were assessed using a two-way ANOVA, and further compared with the Bonferroni post hoc test, at a minimum confidence level of $p < 0.05$.

Results

Expression patterns of GIRK channels in postnatal development

We used the histoblot technique to determine the regional distribution and expression levels of GIRK channel subunits in the brain during postnatal development and in adults. This method is a reliable and convenient way to compare the regional distribution of different proteins in brain samples without compromising the integrity of antibody-binding sites by tissue fixation, which is required for conventional immunocytochemistry (Jo *et al*., 2006; Kopniczky *et al*., 2005; Tönnes *et al.*, 1999). Proteins transferred to nitrocellulose membranes were immunostained with the purified GIRK channel subunit-specific antibodies using conventional immunoblotting. In adult brain (P60), the overall expression patterns of GIRK1, GIRK2 and GIRK3 subunits were rather similar (Figs 1A and 2A), with strong immunoreactivities in the neocortex, cerebellum, hippocampus and thalamus (Figs 1B and C, and 2B). Faint staining was observed in midbrain nuclei, including the inferior and superior colliculus, and brainstem nuclei (Figs 1A and 2A). Very weak staining was observed in basal ganglia nuclei such as the caudate putamen and globus pallidus (Figs 1A and 2A).

The GIRK1-3 proteins were expressed in the developing brain from the day of birth (P0), showing some differences in a region- and subunit-specific manner (Figs 1 and 2). In the cerebellum, the expression of GIRK1 was low in the molecular layer at P5, increased at P10 and then decreased from P15 to adulthood (Fig. 1A and B). In contrast, GIRK1 levels increased steadily in the granule cell layer (Fig. 1A and B). The expression of GIRK2 was highest in the molecular and granule cell layers at P5, and then decreased until adulthood (Fig. 1A and C). In the white matter, the expression for both GIRK1 and GIRK2 was consistently lower than in the molecular and granule cell layers, showing its highest expression at P5, and then decreasing until adulthood (Fig. 1A-C). The expression of GIRK3 increased from its lowest expression at P5 to a peak at P60 (Fig. 2A and B).

Labelling for GIRK1 in the hippocampus was weak at P0 (Fig. 1A) and more detectable at P5 (Fig. 1A), whereas it appeared only around P10 for GIRK2 and became strong at P15 (Fig. 1A). The first labelling for GIRK3 in the hippocampus was detected weakly at P5 and increased steadily until P60 (Fig. 2A). Densitometric measurements performed in the hippocampus demonstrated that, at all developmental stages, immunoreactivity for GIRK1, GIRK2 and GIRK3 was generally greatest within the CA1 region, CA3 region and molecular layer of the dentate gyrus, and lowest in the hilus (Figs 1B and C, and 2B). Furthermore, in all of those subregions of the hippocampus, GIRK1 and GIRK3 proteins increased from the lowest levels at P5-P10 to the highest level at P60, whereas GIRK2 expression remained relatively consistent, with only minor increases early on and levelling out after P15.

Regulation of GIRK1 in the brain of GIRK2-deficient mice

Given the association of GIRK channel subunits in the cerebellum and hippocampus (Aguado *et al.*, 2008; Fernández-Alacid *et al.*, 2009; Koyrakh *et al.*, 2005), one might predict that, as in other hetero-oligomeric ion channels (Ball *et al.*, 2010), the loss of a given subunit would affect the expression and/or turnover of other subunits. We addressed this issue in quantitative histoblotting experiments involving only adult GIRK2 null mice (Fig. 3). In the cerebellum, GIRK1 was reduced in both the molecular (11 ± 1%; $p < 0.05$) and granule cell (30 ± 2%; $p < 0.05$) layers. In the hippocampus, GIRK1 was lower in the CA1 (50 ± 4%, $p < 0.05$), CA3 (34 ± 3%, $p < 0.05$) and molecular layer of the DG (18 ± 1%; $p < 0.05$), but was normal in the hilus (Fig. 3A, C and E). GIRK1 levels were also lower in the caudate putamen (8 ± 1%, $p < 0.05$). Thus, we found that the GIRK1 subunit was consistently and significantly down-regulated in the GIRK2 null mice, although this regulation was different depending on the brain region and the layer or subfield of each region.

Maturation of the expression for GIRK subunits

To determine the distribution and subcellular profile of GIRK1, GIRK2 and GIRK3 distribution during postnatal development, light microscopy immunohistochemical analyses were performed in the hippocampus, as it displayed among the highest immunoreactivity for all three GIRK channel subunits (Fig. 4).

GIRK1—At birth (P0), we observed that GIRK1 was extensively expressed in the somata of principal cells in all hippocampal areas, whereas very weak labelling was detected in the dendritic layers (Fig. 4A1). At P5, GIRK1 immunoreactivity was intensely expressed in principal cell somata, and moderate labelling was detected in the dendritic layers (Fig. 4A2). During the second postnatal week (P10), immunolabelling for GIRK1 was still observed in principal cell somata but more intense labelling was found in the *stratum lacunosum–moleculare* of the CA1 and CA3 regions, and molecular layer of the dentate gyrus (Fig. 4A2). However, during the third postnatal week (P15), a dramatic decrease in GIRK1 immunoreactivity was detected in the principal cell layers throughout the hippocampus (Fig. 4A4). Overall, the distribution of GIRK1 in the hippocampal formation did not change from P21 to P60 (Fig. 4A5 and A6). In the CA1 region, immunolabelling for GIRK1 was strong in the *stratum lacunosum–moleculare*, whereas the *stratum radiatum* showed an uneven labelling with moderate intensity in the proximal half and high intensity in the distal half, and the *stratum oriens* showed moderate intensity (Fig. 4A5 and A6). In the CA3 region, GIRK1 immunoreactivity was strongest in the *strata oriens*, *radiatum* and *lacunosum–moleculare*, whereas the *stratum lucidum* displayed more moderate expression (Fig. 4A5 and A6). In the dentate gyrus, GIRK1 immunoreactivity was strong in the molecular layer and weak in the hilus (Fig. 4A5 and A6). In the pyramidal and granule cell layers, no labelling was observed.

GIRK2—At P0 and P5, GIRK2 was expressed intensely in the principal cells of all hippocampal subregions, with stronger labelling seen in the dendritic layers (Fig. 4B1 and B2) as compared with GIRK1. During the second postnatal week (P10), principal cell layers of areas CA1 and CA3, and the dentate gyrus displayed relatively weak labelling, whereas more intense labelling was found in the dendritic layers, particularly in the CA3 and molecular layer of dentate (Fig. 4B3). At P15 and P21, the pattern of GIRK2 immunolabelling was similar, but stronger than that observed at P10, only showing a stronger signal in the *stratum lacunosum–moleculare* of the CA1 region (Fig. 4B4 and B5). At P60, immunolabelling for GIRK2 was strong in the *stratum lacunosum–moleculare* in the CA1 region, whereas the *stratum radiatum* showed an uneven labelling with moderate intensity in the proximal half and high intensity in the distal half, and the *stratum oriens*

showed moderate intensity (Fig. 4B6). In the CA3 region, GIRK2 immunoreactivity was strongest in the *strata oriens*, *radiatum* and *lacunosum–moleculare*, compared with the more moderate expression in the *stratum lucidum* (Fig. 4B5 and B6). Additionally, in the dentate gyrus, strong GIRK2 immunoreactivity was again detected in the molecular layer and weaker labelling was observed in the hilus (Fig. 4BA6. No labelling was observed in the pyramidal and granule cell layers of the dentate.

GIRK3—At birth (P0), GIRK3 was expressed intensely in the principal cells of all hippocampal areas, whereas very weak labelling was detected in the dendritic layers (Fig. 4C1). At P5, the distribution pattern of GIRK3 changed dramatically, showing a decrease in the pyramidal cell layer and strong expression in the neuropil of all dendritic layers, with the strongest labelling seen in the *stratum lucidum* in the CA3 region (Fig. 4C2). A similar pattern, albeit with greater intensity, of GIRK3 immunolabelling was observed during the second (P10) and third (P5) postnatal week compared with P5 (Fig. 4C3 and C4). However, at P15, intense GIRK3 labelling was also observed in the inner third of the molecular layer in the dentate gyrus (Fig. 4C4). At P21, GIRK3 immunolabelling was observed in the neuropil of all dendritic layers, with the strongest intensity occurring in the *stratum lucidum* in the CA3 region and *stratum lacunosum–moleculare* of the CA1 region (Fig. 4C5). At P60, the distribution of GIRK3 immunolabelling was of similar intensity throughout the neuropil of all dendritic layers in the CA1 region, CA3 region and dentate gyrus, with the strongest intensity in the *stratum lucidum* in the CA3 region and hilus of the dentate gyrus (Fig. 4C6).

Developmental shift in the subcellular localization of GIRK subunits

To investigate in greater detail the changes in the subcellular localization of GIRK channel subunits in CA1 pyramidal neurons throughout postnatal development (P5, P15 and P60), we next carried out electron microscopic studies using the pre-embedding and postembedding immunogold techniques, allowing us to evaluate the subcellular localization at extrasynaptic and synaptic sites, respectively.

Extrasynaptic GIRK-containing channels—We used the pre-embedding immunogold technique to determine the developmental changes in the subcellular localization of GIRK1, GIRK2 and GIRK3 at extrasynaptic sites (Figs 5 and 6). Distribution was quantified in the *stratum radiatum* for the three subunits at P5, P15 and P60. At P5, labelling for GIRK1 (Fig. 5A, B and H), GIRK2 (Fig. 5E and I) and GIRK3 (Fig. 6A, B and H) was found to be primarily associated with the endoplasmic reticulum of dendritic shafts and spine apparatus (75, 71 and 78% of all particles examined for GIRK1, GIRK2 and GIRK3, respectively). Of the immunoparticles found in the plasma membrane, most (82% of GIRK1, 81% of GIRK2 and 52% of GIRK3) were found in postsynaptic compartments, whereas the remainder (18% of GIRK1, 19% of GIRK2 and 48% of GIRK3) were found at presynaptic sites in axon terminals establishing asymmetrical synapses with dendritic spines (Figs 5H and I, and 6H).

At P15, labelling for GIRK1 (Fig. 5C and H), GIRK2 (Fig. 5F and I) and GIRK3 (Fig. 6C, D and H) was found at both intracellular sites in dendritic shafts and spines (51, 49 and 62% of all particles examined for GIRK1, GIRK2 and GIRK3, respectively), and along the plasma membrane, where most (82% of GIRK1, 83% of GIRK2 and 57% of GIRK3) were found in postsynaptic compartments, and the rest (18% of GIRK1, 17% of GIRK2 and 43% of GIRK3) were found at presynaptic sites in axon terminals establishing asymmetrical synapses with dendritic spines (Figs 5H and I, and 6H). Finally, at P60, labelling for GIRK1 (Fig. 5D and H), GIRK2 (Fig. 5G and I) and GIRK3 (Fig. 6E-F and H) was found primarily along the plasma membrane, and less at intracellular sites (38, 35 and 46% of all particles examined for GIRK1, GIRK2 and GIRK3, respectively). Along the plasma membrane, most

immunoparticles (84% of GIRK1, 86% of GIRK2 and 69% of GIRK3) were found in postsynaptic compartments, and the remainder (16% of GIRK1, 14% of GIRK2 and 31% of GIRK3) in axon terminals (Figs 5H and I, and 6H). Immunoparticles for GIRK3 were also found at mossy fibre terminals in the CA3 region of the hippocampus (Fig. 6G).

As dendritic spines are the compartments showing the highest expression for GIRK, in order to determine the abundance of the three subunits in the spines located in the different dendritic subfields of CA1, we next analysed their plasma membrane distribution as a function of distance from the soma in the adult (immunoparticles/μm^2; Table 1). The density of GIRK1 and GIRK2 followed a similar pattern; it was low in spines present in the proximal part of the *stratum radiatum*, increased significantly in the distal part of the *stratum radiatum* and was highest in the *stratum lacunosum–moleculare* (Table 1). In contrast, the density of GIRK3 was similar in the three hippocampal subfields and significantly different from that of GIRK1 and GIRK2 (Table 1).

Synaptic GIRK-containing channels—To evaluate the developmental expression profile of synaptic GIRK-containing channels, we performed quantitative postembedding immunogold labelling, and examined GIRK1, GIRK2 and GIRK3 at asymmetric synapses of CA1 pyramidal neurons in the *stratum radiatum* during postnatal development (Table 2). GIRK1 was detected at perisynaptic and/or extrasynaptic sites of the dendritic spines but never along the main body of the postsynaptic density (PSD) at any developmental age analysed (Fig. 7A-C). GIRK2 and GIRK3, however, were observed along the PSD at all developmental ages, each displaying different patterns. At P5, GIRK2 immunoparticles were detected at low levels along the PSD (1.03 ± 0.11 immunoparticles/labelled synapse; Fig. 7D; Table 2), increased by P15 (1.84 ± 0.11 immunoparticles/labelled synapse, $p < 0.05$; Fig. 7E) and were highest at P60 (2.51 ± 0.12 immunoparticles/labelled synapse, $p < 0.05$; Fig. 7F). In contrast, we observed a similar number of GIRK3 immunoparticles per synapse and percentage of synapses labelled at all ages studied (P5, 1.47 ± 0.11 immunoparticles/labelled synapse; P15, 1.53 ± 0.11 immunoparticles/labelled synapse; P60, 1.54 ± 0.12 immunoparticles/labelled synapse; Fig. 7G-I, Table 2). We used anti-PSD-95 and anti-GluN1 antibodies as controls for postembedding experiments at each developmental age and always found three to four times more immunoparticles (not shown) than those for anti-GIRK antibodies, suggesting no technical limitations.

Discussion

In this work, we used a combination of different techniques to reveal the temporal and spatial expression profile and subcellular localization of three GIRK channel subunits in the rodent brain during postnatal development. The results obtained with histoblot suggest that GIRK1, GIRK2 and GIRK3 are widely distributed in the adult brain and during the early stages of development, and display an overlapping and prominent expression pattern during development in multiple brain regions including the hippocampus, cerebellum, neocortex and thalamus. In addition, immunoelectron microscopy combined with quantitative analysis revealed that the subcellular distribution of GIRK channel subunits is differentially localized in a subunit- and time-dependent manner within the developing hippocampus. Specifically, we have provided evidence for the existence of a similar distribution pattern for GIRK1 and GIRK2, which is different from that for GIRK3. These data demonstrate that the three GIRK channel subunits are differentially regulated and their co-localization begins in the early stages of development.

Expression of GIRK channel subunits during brain development

Unravelling the spatial and temporal appearance of the channel subunits is important to understand the molecular basis of GIRK signalling. In the adult, native GIRK channels are believed to be composed of either homomeric assemblies of GIRK2 (Jelacic *et al.*, 2000; Koyrakh *et al.*, 2005) or heteromeric complexes of GIRK1, GIRK2 and/or GIRK3 subunits (Chen *et al.*, 1997; Karschin *et al.*, 1996; Kobayashi *et al.*, 1995). There is general agreement that GIRK2 is an integral subunit in most neuronal GIRK channels and GIRK1/GIRK2 heteromultimers are widely considered to be the prototypical GIRK channel in the brain (Cruz *et al.*, 2004; Koyrakh *et al.*, 2005; Lüscher *et al.*, 1997; Marker *et al.*, 2005, 2006; Torrecilla *et al.*, 2002). The loss of GIRK1 staining that we have detected in a number of brain regions, as well as in different layers or subfields within a specific region, in GIRK2 knockout mice supports this contention, as has also been suggested previously (Koyrakh *et al.*, 2005; Liao *et al.*, 1996; Torrecilla *et al.*, 2002). Nevertheless, the expression of GIRK2 does not preclude the formation of signalling complexes that do not contain the GIRK2 subunit, as we know that neurons produce more than one type of GIRK channel (Luján *et al.*, 2009). This is clearly illustrated in the cerebellum by the existence of GIRK channels that do not contain the GIRK2 subunit (Aguado *et al.*, 2008). Therefore, regional differences in the expression of GIRK subunits may serve as an indicator for the presence of distinct GIRK channel subtypes. This is important because differential subunit assembly can confer distinct GIRK channel properties (Duprat *et al.*, 1995; Krapivinsky *et al.*, 1995).

In the present study, we have shown by histoblot that GIRK1, GIRK2 and GIRK3 are widely expressed in both the developing and adult brain, in agreement with previous *in-situ* hybridization studies (Chen *et al.*, 1997; Karschin *et al.*, 1996; Karschin & Karschin, 1997). In the hippocampus, we found similar temporal expression patterns for GIRK1, GIRK2 and GIRK3 in all hippocampal subfields and dendritic layers, increasing progressively during postnatal development to reach adult levels. In general, GIRK protein expression during development correlated well with the corresponding mRNA pattern (Karschin & Karschin, 1997; Chen *et al.*, 1997), suggesting that transcriptional regulation is an important determinant of the density of GIRK channel subunits in hippocampal neurons.

However, the larger spatial resolution of the histoblot technique compared with immunoblot allowed us to detect marked differences in the level of immunoreactivity and expression profiles in a layer-specific manner in the cerebellum. Thus, the expression of GIRK2 decreased progressively with age, whereas the expression of GIRK1 and GIRK3 increased progressively during postnatal development to reach adult levels. The exception was the expression of GIRK1 in the molecular layer, which increased by P10 and then decreased following a similar pattern as GIRK2. Given that GIRK1 and GIRK2 are mainly expressed in cerebellar granule cells (Aguado *et al.*, 2008; Ciruela *et al.*, 2010), their similar expression pattern in the molecular layer during the first and second postnatal week indicates that they are co-expressed in granule cells migrating from the external to the internal granular layer, in agreement with previous immunohistochemical studies in the cerebellum (Slesinger *et al.*, 1996). Although GIRK3 is also expressed in granule cells (Aguado *et al*., 2008; Ciruela *et al*., 2010), its differential expression pattern in the molecular layer probably indicates its steady-state expression profile in Purkinje cells, the cell type showing the highest expression level for this subunit (Aguado *et al.*, 2008).

Differential subcellular localization of extrasynaptic GIRK channel subunits in the developing hippocampus

The development of the hippocampal network requires neuronal activity, which is shaped by the differential expression and sorting of a variety of neurotransmitter receptors and ion channels. Parallel to their maturation, hippocampal neurons undergo a distinct development

of their neurotransmitter receptor/ion channel profiles. Specific neurotransmitter receptors and ion channel subunits are developmentally regulated in the hippocampus, in a parallel process in the establishment and maturation of synaptic contacts (Luján *et al*., 2005). However, data regarding the exact temporal expression of GIRK channels are scarce. Here, the use of high-resolution immunoelectron microscopy yielded novel findings about the differential trafficking of GIRK1, GIRK2 and GIRK3 to the dendritic compartments as a function of age. Thus, during the first week of postnatal development, GIRK1 and GIRK2 were largely expressed in the somata of CA1 pyramidal neurons, almost entirely intracellular in association with the rough endoplasmic reticulum. This early postnatal distribution was distinct from later stages when GIRK1 and GIRK2 migrate into dendritic shafts and spines of CA1 pyramidal neurons, and in the adult they are mainly localized to spines (Koyrakh *et al*., 2005), consistent with previous studies (Drake *et al.*, 1997; Lüscher *et al.*, 1997; Ponce *et al.*, 1996). Although GIRK3 generally followed this spatial and temporal distribution pattern at postsynaptic sites, it appears to have a preferential localization at presynaptic sites in glutamatergic terminals establishing synapses with CA1 neurons during development, as also suggested in culture neurons (Grosse *et al.*, 2003). This presynaptic localization of GIRK channel subunits is consistent with previous morphological (Marker *et al.*, 2005; Morishige *et al*., 1996; Ponce *et al.*, 1996) and functional (Fernández-Alacid *et al*., 2009) observations, although the relevance of GIRK3 in axon terminals in the hippocampus is still unknown.

The well-characterized laminar arrangement of the cell bodies of CA1 pyramidal cells in the adult hippocampus allowed us to investigate changes in the density of GIRK expression in dendritic spines as a function of distance from the soma in the adult. Quantitative comparison of immunogold densities showed that GIRK1 and GIRK2 followed a similar proximal-to-distal gradient in the hippocampal pyramidal cells, but GIRK3 did not show such a gradient. These differential expression patterns may contribute significantly to changes that determine the properties of GIRK channels and thereby influence different hippocampal function. Indeed, our data are consistent with previous electrophysiological studies showing that, in CA1 neurons from GIRK3 knockout mice, no differences in baclofen-evoked current relative to wild-type were observed (Koyrakh *et al.*, 2005). Thus, GIRK3-containing channels seem to play only a modest role in the postsynaptic inhibitory effects of $GABA_B$ receptor stimulation (Koyrakh *et al.*, 2005). In addition, the strikingly similar extrasynaptic distribution of GIRK1 and GIRK2 is reminiscent of the distribution of the $GABA_B$ receptor (Koyrakh *et al.*, 2005; López-Bendito *et al.*, 2004). Therefore, given our data, it seems reasonable to suggest that GIRK channels consisting of GIRK1 and GIRK2 mediate the dominant component of the $GABA_B$-mediated postsynaptic inhibition.

Segregation of synaptic GIRK channel subunits in the developing hippocampus

One important finding emerging from our data is that GIRK channel subunits are also regulated at synaptic sites during development. Indeed, we show here that excitatory PSDs exhibit profound changes in relative protein composition and abundance of GIRK2 during development. In contrast, the GIRK1 subunit was never detected at synaptic sites and the GIRK3 subunit levels were constant throughout postnatal development. The absence of GIRK1 in the postsynaptic specialization during development and adulthood is additional evidence of the molecular diversity of GIRK channels in the central nervous system and is consistent with observations in other brain regions (Fernández-Alacid *et al.*, 2009; Koyrakh *et al*., 2005; Marker *et al.*, 2005). Our data suggest that GIRK channels within the synaptic specialization are likely to be GIRK2/GIRK3 heterotetramers. This specific distribution of GIRK channels within the PSDs may reflect the presence of a PSD-95, Dlg and ZO-1 (PDZ) interaction motif on the GIRK2c splice isoform and/or GIRK3 (Inanobe *et al*., 1999; Nehring *et al.*, 2000; Kurachi & Ishii, 2004). At present, the functional significance of GIRK

channels within the synaptic specialization is unknown, but they might be activated by $GABA_B$ receptors, which are known to be also present at excitatory synapses in CA1 pyramidal cells (Kulik *et al.*, 2006).

In conclusion, although our data support the contention that heteromeric GIRK1/GIRK2 channels are the prevalent GIRK channels in the developing and adult hippocampus, subpopulations of GIRK channels with distinct subunit composition and subcellular distribution can be discerned. Moreover, this study reveals striking developmental regulation of both the expression and subcellular distribution of neuronal GIRK channel subunits. Molecular, developmental and subcellular diversity in the neuronal GIRK channel repertoire may afford an opportunity for the selective modulation of distinct subpopulations of GIRK channels, an approach that could prove useful for the treatment of disorders of neuronal excitability including seizures.

Supplementary Material

Refer to Web version on PubMed Central for supplementary material.

Acknowledgments

We thank members of the laboratories of K.W. and R.L. for comments on the manuscript. We also thank Mrs Mercedes Gil for excellent technical assistance. This work was supported by grants from the Spanish Ministry of Education and Science (BFU-2009-08404/BFI) and CONSOLIDER (CSD2008-00005) to R.L, the NIH (RO1 MH061933 and P50 DA011806) to K.W., and the Medical Research Council UK (G0601509) and the Biotechnology and Biological Sciences Research Council UK (BB/F011326/1) to E.M.

Abbreviations

$GABA_B$	metabotropic γ-aminobutyric acid type B
GIRK	G protein-gated inwardly-rectifying K^+
NGS	normal goat serum
P	postnatal day
PSD	postsynaptic density
TBS	Tris-buffered saline

References

Aguado C, Colón J, Ciruela F, Schlaudraff F, Cabañero MJ, Perry C, Watanabe M, Liss B, Wickman K, Luján R. Cell type-specific subunit composition of G protein-gated potassium channels in the cerebellum. J. Neurochem. 2008; 105:497–511. [PubMed: 18088366]

Ball SM, Atlason PT, Shittu-Balogun OO, Molnár E. Assembly and intracellular distribution of kainate receptors is determined by RNA editing and subunit composition. J Neurosci. 2010; 114:1805–1818.

Chen SC, Ehrhard P, Goldowitz D, Smeyne RJ. Developmental expression of the GIRK family of inward rectifying potassium channels: implications for abnormalities in the weaver mutant mouse. Brain Res. 1997; 778:251–264. [PubMed: 9459542]

Ciruela F, Fernández-Dueñas V, Sahlholm K, Fernández-Alacid L, Nicolau JC, Watanabe M, Luján R. Evidence for oligomerization between GABAB receptors and GIRK channels containing the GIRK1 and GIRK3 subunits. Eur. J. Neurosci. 2010; 32:1265–1277. [PubMed: 20846323]

Cruz HG, Ivanova T, Lunn ML, Stoffel M, Slesinger PA, Lüscher C. Bi-directional effects of GABA(B) receptor agonists on the mesolimbic dopamine system. Nat. Neurosci. 2004; 7:153–159. [PubMed: 14745451]

David M, Richer M, Mamarbachi AM, Villeneuve LR, Dupre DJ, Hebert TE. Interactions between GABA-B1 receptors and kir 3 inwardly rectifying potassium channels. Cell Signal. 2006; 18:2172–2181. [PubMed: 16809021]

Drake CT, Bausch SB, Milner TA, Chavkin C. GIRK1 immunoreactivity is present predominantly in dendrites, dendritic spines, and somata in the CA1 region of the hippocampus. Proc. Natl Acad. Sci. U.S.A. 1997; 94:1007–1012. [PubMed: 9023373]

Duprat F, Lesage F, Guillemare E, Fink M, Hugnot JP, Bigay J, Lazdunski M, Romey G, Barhanin J. Heterologous multimeric assembly is essential for K+ channel activity of neuronal and cardiac G-protein activated inward rectifiers. Biochem. Biophys. Res. Commun. 1995; 212:657–663. [PubMed: 7626080]

Fernández-Alacid L, Aguado C, Ciruela F, Martín R, Colón J, Cabañero MJ, Gassmann M, Watanabe M, Shigemoto R, Wickman K, Bettler B, Sánchez-Prieto J, Luján R. Subcellular compartment-specific molecular diversity of pre- and post-synaptic GABA-activated GIRK channels in Purkinje cells. J. Neurochem. 2009; 110:1363–1376. [PubMed: 19558451]

Fowler CE, Aryal P, Suen KF, Slesinger PA. Evidence for association of GABA(B) receptors with Kir3 channels and regulators of G protein signalling (RGS4) proteins. J. Physiol. 2007; 580:51–65. [PubMed: 17185339]

Grosse G, Eulitz D, Thiele T, Pahner I, Schroter S, Takamori S, Grosse J, Wickman K, Tapp R, Veh RW, Ottersen OP, Ahnert-Hilger G. Axonal sorting of Kir3.3 defines a GABA-containing neuron in the CA3 region of rodent hippocampus. Mol. Cell. Neurosci. 2003; 24:709–724. [PubMed: 14664820]

Inanobe A, Yoshimoto Y, Horio Y, Morishige KI, Hibino H, Matsumoto S, Tokunaga Y, Maeda T, Hata Y, Takai Y, Kurachi Y. Characterization of G-protein-gated K+ channels composed of Kir3.2 subunits in dopaminergic neurons of the substantia nigra. J. Neurosci. 1999; 19:1006–1017. [PubMed: 9920664]

Jelacic TM, Kennedy ME, Wickman K, Clapham DE. Functional and biochemical evidence for G-protein-gated inwardly rectifying K+ (GIRK) channels composed of GIRK2 and GIRK3. J. Biol. Chem. 2000; 275:36211–36216. [PubMed: 10956667]

Jo J, Ball SM, Seok H, Oh S-B, Massey PV, Molnar E, Bashir ZI, Cho K. Experience-dependent modification of mechanisms of long-term depression. Nat. Neurosci. 2006; 9:170–172. [PubMed: 16429132]

Jones KA, Borowsky B, Tamm JA, Craig DA, Durkin MM, Dai M, Yao WJ, Johnson M, Gunwaldsen C, Huang LY, Tang C, Shen Q, Salon JA, Morse K, Laz T, Smith KE, Nagarathnam D, Noble SA, Branchek TA, Gerald C. GABA(B) receptors function as a heteromeric assembly of the subunits GABA(B)R1 and GABA(B)R2. Nature. 1998; 396:674–679. [PubMed: 9872315]

Karschin C, Dissmann E, Stuhmer W, Karschin A. IRK(1–3) and GIRK(1–4) inwardly rectifying K+ channel mRNAs are differentially expressed in the adult rat brain. J. Neurosci. 1996; 16:3559–3570. [PubMed: 8642402]

Karschin C, Karschin A. Ontogeny of gene expression of Kir channel subunits in the rat. Mol. Cell. Neurosci. 1997; 10:131–148. [PubMed: 9532576]

Kobayashi T, Ikeda K, Ichikawa T, Abe S, Togashi S, Kumanishi T. Molecular cloning of a mouse G-protein-activated K+ channel (mGIRK1) and distinct distributions of three GIRK (GIRK1, 2 and 3) mRNAs in mouse brain. Biochem. Biophys. Res. Commun. 1995; 208:1166–1173. [PubMed: 7702616]

Kopniczky Z, Dobó E, Borbély S, Világi I, Détári L, Krisztin-Péva B, Bagosi A, Molnár E, Mihály A. Lateral entorhinal cortex lesions rearrange afferents, glutamate receptors, increase seizure latency and suppress seizure-induced c-fos expression in the hippocampus of adult rat. J. Neurochem. 2005; 95:111–124. [PubMed: 16181416]

Koyrakh L, Luján R, Colon J, Karschin C, Kurachi Y, Karschin A, Wickman K. Molecular and cellular diversity of neuronal G-protein-gated potassium channels. J. Neurosci. 2005; 25:11468–11478. [PubMed: 16339040]

Krapivinsky G, Gordon EA, Wickman K, Velimirović B, Krapivinsky L, Clapham DE. The G-protein-gated atrial K+ channel IKACh is a heteromultimer of two inwardly rectifying K+-channel proteins. Nature. 1995; 374:135–141. [PubMed: 7877685]

Kulik A, Vida I, Fukazawa Y, Guetg N, Kasugai Y, Marker CL, Rigato F, Bettler B, Wickman K, Frotscher M, Shigemoto R. Compartment dependent colocalization of Kir3.2-containing K^+-channels and GABAB receptors in hippocampal pyramidal cells. J. Neurosci. 2006; 26:4289–4297. [PubMed: 16624949]

Kurachi Y, Ishii M. Cell signal control of the G protein-gated potassium channel and its subcellular localization. J. Physiol. 2004; 554:285–294. [PubMed: 12923211]

Labouèbe G, Lomazzi M, Cruz HG, Creton C, Luján R, Li M, Yanagawa Y, Obata K, Watanabe M, Wickman K, Boyer SB, Slesinger PA, Lüscher C. RGS2 modulates coupling between GABAB receptors and GIRK channels in dopamine neurons of the ventral tegmental area. Nat. Neurosci. 2007; 10:1559–1568. [PubMed: 17965710]

Lesage F, Guillemare E, Fink M, Duprat F, Heurteaux C, Fosset M, Romey G, Barhanin J, Lazdunski M. Molecular properties of neuronal G-protein-activated inwardly rectifying K+ channels. J. Biol. Chem. 1995; 270:28660–28667. [PubMed: 7499385]

Liao YJ, Jan YN, Jan LY. Heteromultimerization of G-protein-gated inwardly rectifying K+ channel proteins GIRK1and GIRK2 and their altered expression in weaver brain. J. Neurosci. 1996; 16:7137–7150. [PubMed: 8929423]

López-Bendito G, Shigemoto R, Kulik A, Vida I, Fairén A, Luján R. Distribution of metabotropic GABA receptor subunits GABAB1a/b and GABAB2 in the rat hippocampus during prenatal and postnatal development. Hippocampus. 2004; 14:836–848. [PubMed: 15382254]

Luján R., Nusser Z.; Roberts, JD.; Shigemoto, R.; Somogyi, P. Perisynaptic location of metabotropic glutamate receptors mGluR1 and mGluR5 on dendrites and dendritic spines in the rat hippocampus. Eur. J. Neurosci. 1996; 8:1488–1500. [PubMed: 8758956]

Luján R, Shigemoto R, López-Bendito G. Glutamate and GABA receptor signalling in the developing brain. Neuroscience. 2005; 130:567–580. [PubMed: 15590141]

Luján R, Shigemoto R. Localization of metabotropic GABA receptor subunits GABAB1 and GABAB2 relative to synaptic sites in the rat developing cerebellum. Eur. J. Neurosci. 2006; 23:1479–1490. [PubMed: 16553611]

Luján R, Maylie J, Adelman JP. New sites of action for GIRK and SK channels. Nat. Rev. Neurosci. 2009; 10:475–480. [PubMed: 19543219]

Lüscher C, Jan LY, Stoffel M, Malenka RC, Nicoll RA. G protein-coupled inwardly rectifying K+ channels (GIRKs) mediate postsynaptic but not presynaptic transmitter actions in hippocampal neurons. Neuron. 1997; 19:687–695. [PubMed: 9331358]

Lüscher C, Slesinger PA. Emerging roles for G protein-gated inwardly rectifying potassium (GIRK) channels in health and disease. Nat. Rev. Neurosci. 2010; 11:301–315. [PubMed: 20389305]

Ma D, Zerangue N, Raab-Graham K, Fried SR, Jan YN, Jan LY. Diverse trafficking patterns due to multiple traffic motifs in G protein-activated inwardly rectifying potassium channels from brain and Herat. Neuron. 2002; 33:715–729. [PubMed: 11879649]

Marker CL, Stoffel M, Wickman K. Spinal G-protein-gated K+ channels formed by GIRK1 and GIRK2 subunits modulate thermal nociception and contribute to morphine analgesia. J. Neurosci. 2004; 24:2806–2812. [PubMed: 15028774]

Marker C, Luján R, Colón J, Wickman K. Distinct populations of spinal cord lamina II interneurons expressing G-protein gated potassium channels. J. Neurosci. 2006; 26:12251–12259. [PubMed: 17122050]

Morishige KI, Inanobe A, Takahashi N, Yoshimoto Y, Kurachi H, Miyake A, Tokunaga Y, Maeda T, Kurachi Y. G protein-gated K+ channel (GIRK1) protein is expressed presynaptically in the paraventricular nucleus of the hypothalamus. Biochem. Biophys. Res. Commun. 1996; 220:300–305. [PubMed: 8645300]

Nehring RB, Wischmeyer E, Doring F, Veh RW, Sheng M, Karschin A. Neuronal inwardly rectifying K(+) channels differentially couple to PDZ proteins of the PSD-95/SAP90 family. J. Neurosci. 2000; 20:156–162. [PubMed: 10627592]

Ponce A, Bueno E, Kentros C, Vega-Saenz de Miera E, Chow A, Hillman D, Chen S, Zhu L, Wu MB, Wu X, Rudy B, Thornhill WB. G-protein-gated inward rectifier K+ channel proteins (GIRK1) are present in the soma and dendrites as well as in nerve terminals of specific neurons in the brain. J Neurosci. 1996; 16:1990–2001. [PubMed: 8604043]

Perry CA, Pravetoni M, Teske JA, Aguado C, Erickson DJ, Medrano JF, Luján R, Kotz CM, Wickman K. Predisposition to late-onset obesity in GIRK4 knockout mice. Proc. Natl Acad. Sci. U.S.A. 2008; 105:8148–8153. [PubMed: 18523006]

Slesinger PA, Patil N, Liao J, Jan YN, Jan LY, Cox DR. Functional effects of the mouse weaver mutation on G protein-gated inwardly rectifying K+ channels. Neuron. 1996; 16:321–331. [PubMed: 8789947]

Slesinger P, Stoffel M, Jan Y, Jan L. Defective γ-aminobutyric acid type B receptor-activated inwardly rectifying K+ currents in cerebellar granule cells isolated from weaver and Girk2 null mutant mice. Proc. Natl Acad. Sci. U.S.A. 1997; 94:12210–12217. [PubMed: 9342388]

Tonnes J, Stierli B, Cerletti C, Behrmann JT, Molnar E, Streit P. Regional distribution and developmental changes of GluR1-flop protein revealed by monoclonal antibody in rat brain. J. Neurochem. 1999; 73:2195–2205. [PubMed: 10537080]

Torrecilla M, Marker CL, Cintora SC, Stoffel M, Williams JT, Wickman K. G-protein-gated potassium channels containing Kir3.2 and Kir3.3 subunits mediate the acute inhibitory effects of opioids on locus ceruleus neurons. J. Neurosci. 2002; 22:4328–4334. [PubMed: 12040038]

Vigot R, Barbieri S, Brauner-Osborne H, Turecek R, Shigemoto R, Zhang YP, Luján R, Jacobson LH, Biermann B, Fritschy JM, Vacher CM, Müller M, Sansig G, Guetg N, Cryan JF, Kaupmann K, Gassmann M, Oertner TG, Bettler B. Differential compartmentalization and distinct functions of GABAB receptor variants. Neuron. 2006; 50:589–601. [PubMed: 16701209]

Wickman K, Karschin C, Karschin A, Picciotto MR, Clapham DE. Brain localization and behavioral impact of the G-protein-gated K+ channel subunit GIRK4. J. Neurosci. 2000; 20:5608–5615. [PubMed: 10908597]

Wickman K, Pu WT, Clapham DE. Structural characterization of the mouse Girk genes. Gene. 2002; 284:241–250. [PubMed: 11891065]

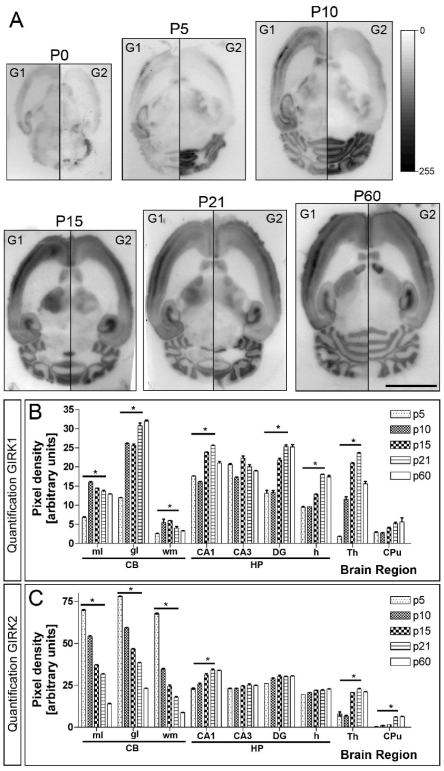

Fig. 1.

Developmental and regional distribution of GIRK1 and GIRK2 subunits in the mouse brain. (A) GIRK protein distribution was visualized on histoblots of brain horizontal sections at various stages of postnatal development using affinity-purified anti-GIRK1 and anti-GIRK2 antibodies. The two GIRK channel subunits exhibited broad and overlapping distributions in the developing and adult brain. In particular, strong immunoreactivity for GIRK1 and GIRK2 was detected in the neocortex, cerebellum, hippocampus and thalamus, with the lowest intensity in the caudate putamen. (B and C) The histoblots were scanned and densitometric measurements from five independent experiments were averaged to compare the protein densities for each developmental time point. Error bars indicate SEM; *p < 0.001 compared with P60. Scale bar, 0.4 cm.

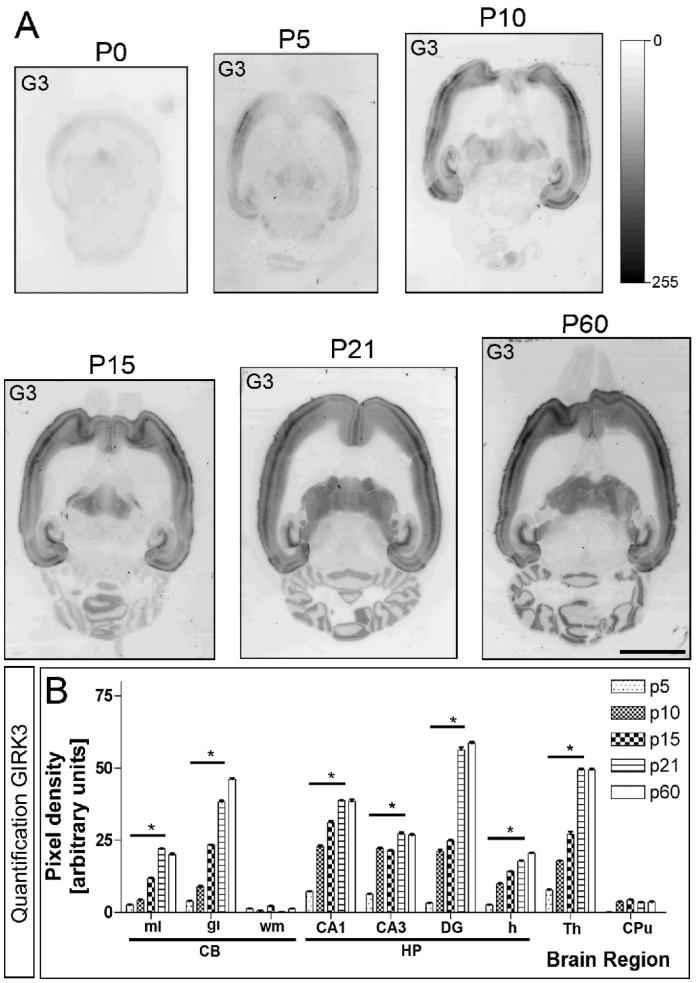

Fig. 2.

Developmental and regional distribution of the GIRK3 subunit in the rat brain. (A) GIRK protein distribution was visualized on histoblots of brain horizontal sections at various stages of postnatal development using affinity-purified anti-GIRK3 antibodies. GIRK3 exhibited a broad distribution pattern in the developing and adult brain. Strong immunoreactivity for GIRK3 was detected in the neocortex, hippocampus, thalamus and cerebellum, with the lowest intensity in the caudate putamen. (B and C) The developed histoblots were scanned and densitometric measurements from five independent experiments were averaged together to compare the protein densities for each age. In all brain regions analysed, as well as in all layers or subfields from each region, the GIRK3 protein increased from its lowest expression at P5 to a peak at P60. Error bars indicate SEM; *$p < 0.001$ compared with P60. Scale bar, 0.4 cm.

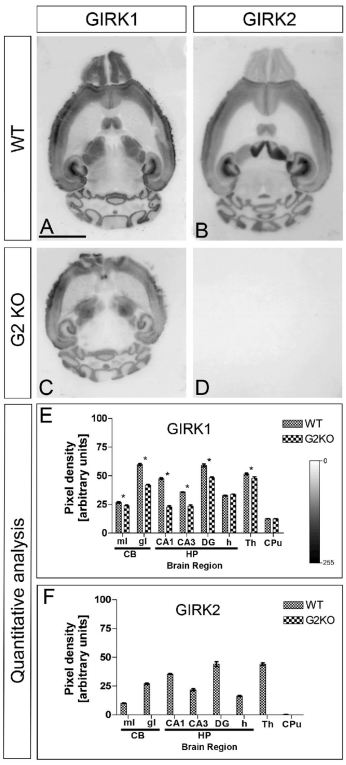

Fig. 3.

Regulation of GIRK1 expression in the brain of GIRK2 null mice. Protein distribution was visualized on histoblots of brain horizontal sections at P60 using affinity-purified anti-GIRK1 antibodies. The developed histoblots were scanned and densitometric measurements from five independent experiments were averaged together to compare the protein densities for each age. (A, C and E) The pattern of expression of GIRK1 observed in the wild-type (A) was consistently reduced in the brain of GIRK2 null mice (C). In all brain regions analysed, as well as in all layers or subfields from each region, the expression of GIRK1 was significantly reduced (E). (B, D and F) GIRK2 immunoreactivity was completely absent in the brain of GIRK2 null mice (D and F), demonstrating the specificity of the antibody. Error bars indicate SEM; *$p < 0.001$ compared with P60 in all cases. Scale bar, 0.5 cm.

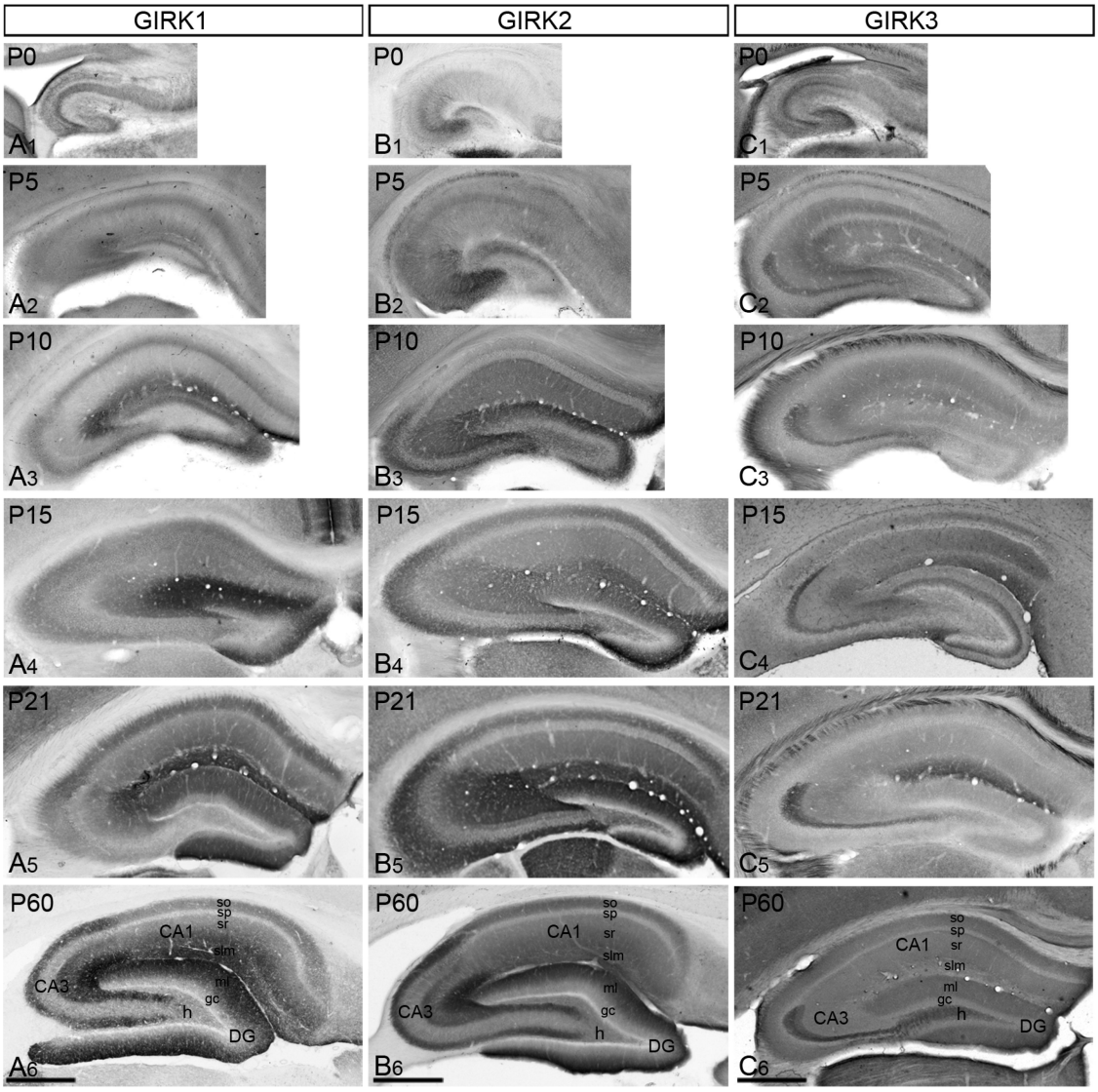

Fig. 4.

Immunoreactivity for GIRK1, GIRK2 and GIRK3 in the hippocampus during postnatal development using a pre-embedding immunoperoxidase method. sp, *stratum pyramidale*; gc, granule cell layer; h, hilus; ml, molecular layer. Scale bar: A-C, 0.5 cm.

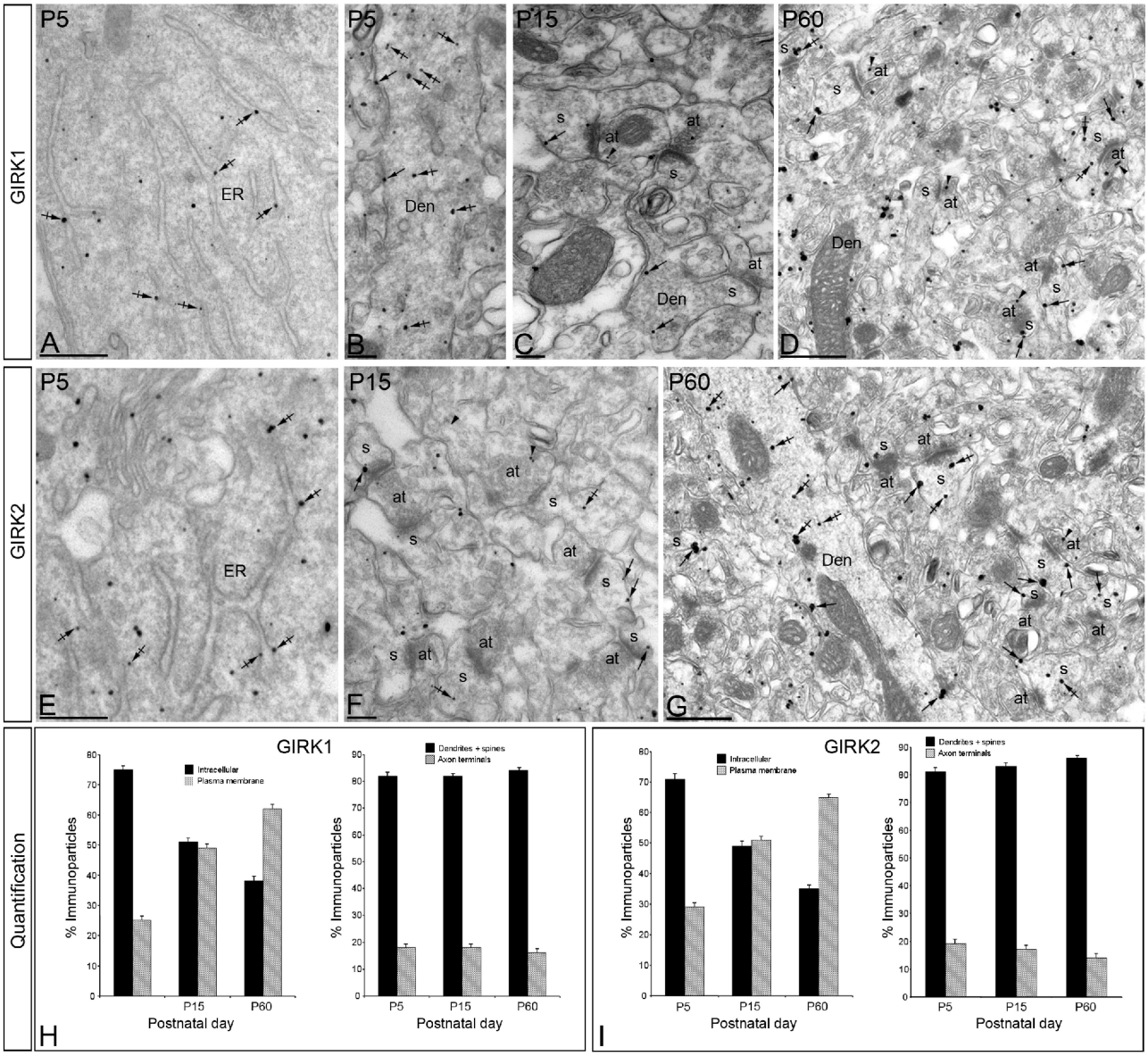

Fig. 5.

Developmental shift in the subcellular localization of GIRK1 and GIRK2. Electron micrographs of the CA1 region of the hippocampus showing immunogold particles for GIRK1 and GIRK2 during postnatal development, as detected using a pre-embedding method. GIRK1 and GIRK2 showed similar distribution patterns throughout development. At P5, immunoparticles for GIRK1 (A) and GIRK2 (E) were mainly associated with the endoplasmic reticulum (ER) in the cytoplasm (crossed arrows) of pyramidal cells. In the *stratum radiatum*, immunoparticles for GIRK1 (B) and GIRK2 (not shown) were mainly detected at intracellular sites (crossed arrows) in the dendritic shafts (Den) of pyramidal cells, and only a few immunoparticles were found along the plasma membrane (arrows). At P15, immunoparticles for GIRK1 (C) and GIRK2 (F) were detected along the plasma membrane (arrows) of dendritic spines (s) shafts (Den) and at intracellular sites (crossed arrows). A few immunoparticles for GIRK and GIRK2 were also found in axon terminals (at) establishing asymmetrical synapses with dendritic spines (s). At P60, immunoparticles

for GIRK1 (D) and GIRK2 (G) were mainly detected at postsynaptic sites along the plasma membrane (arrows) of dendritic spines (s) shafts (Den, arrows) and at intracellular sites (crossed arrows) in associated with membranes in spines (s) and dendrites (Den). In less proportion, immunoparticles for GIRK and GIRK2 were also found in axon terminals (at) establishing asymmetrical synapses with dendritic spines (s). Quantitative analysis showing the percentage of immunoparticles for GIRK1 (H) and GIRK2 (I) at intracellular sites vs. plasma membrane (left histogram) and along the plasma membrane of postsynaptic compartments, such as dendrites, and spines vs. presynaptic compartments, such as axon terminals (right histogram), during postnatal development. Scale bars: A and F, 0.5 μm; B-D, F and G, 0.2 μm.

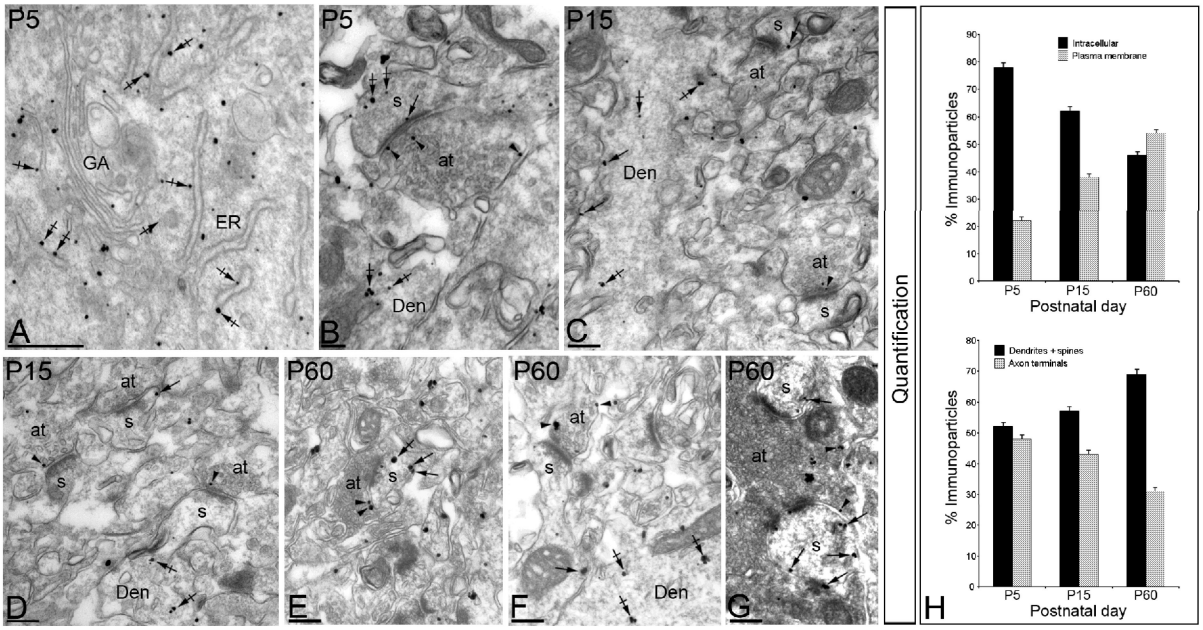

Fig. 6.

Electron micrographs of the CA1 region of the hippocampus showing immunogold particles for GIRK3 during postnatal development, as detected using a pre-embedding method. (A and B) At P5, immunoparticles for GIRK3 were mainly associated with the endoplasmic reticulum (ER) in the cytoplasm (crossed arrows) of pyramidal cells. In the *stratum radiatum* (B), immunoparticles for GIRK3 were mainly detected at presynaptic sites (arrowheads) in axon terminals (at) establishing asymmetrical synapses, as well as at intracellular sites in the dendritic shafts (Den) and spines (s) of pyramidal cells, and only a few immunoparticles were found along the plasma membrane (arrows). (C and D) At P15, immunoparticles for GIRK3 were detected along the plasma membrane (arrows) and intracellular sites (crossed arrows) of dendritic shafts (Den) and spines (s). GIRK3 immunoparticles were also observed in axon terminals (at) (arrowheads) establishing asymmetrical synapses with dendritic spines (s). (E-G) At P60, immunoparticles for GIRK3 were localized along the plasma membrane and intracellular sites of dendritic spines (s) and shafts (Den) (arrows), and along the plasma membrane of axon terminals (at) (arrowheads), in the *stratum radiatum*. In the *stratum lucidum* of the CA3 region, (G), GIRK3 immunoparticles were also observed in mossy fibres (at) (arrowheads) establishing asymmetrical synapses with dendritic spines (s) of pyramidal cells. (H) Quantitative analysis showing the percentage of immunoparticles for GIRK3 at intracellular sites vs. plasma membrane (top histogram) and along the plasma membrane of postsynaptic compartments, such as dendrites, and spines vs. presynaptic compartments, such as axon terminals (bottom histogram), during postnatal development. Scale bars: A, 0.5 μm; B-G, 0.2 μm.

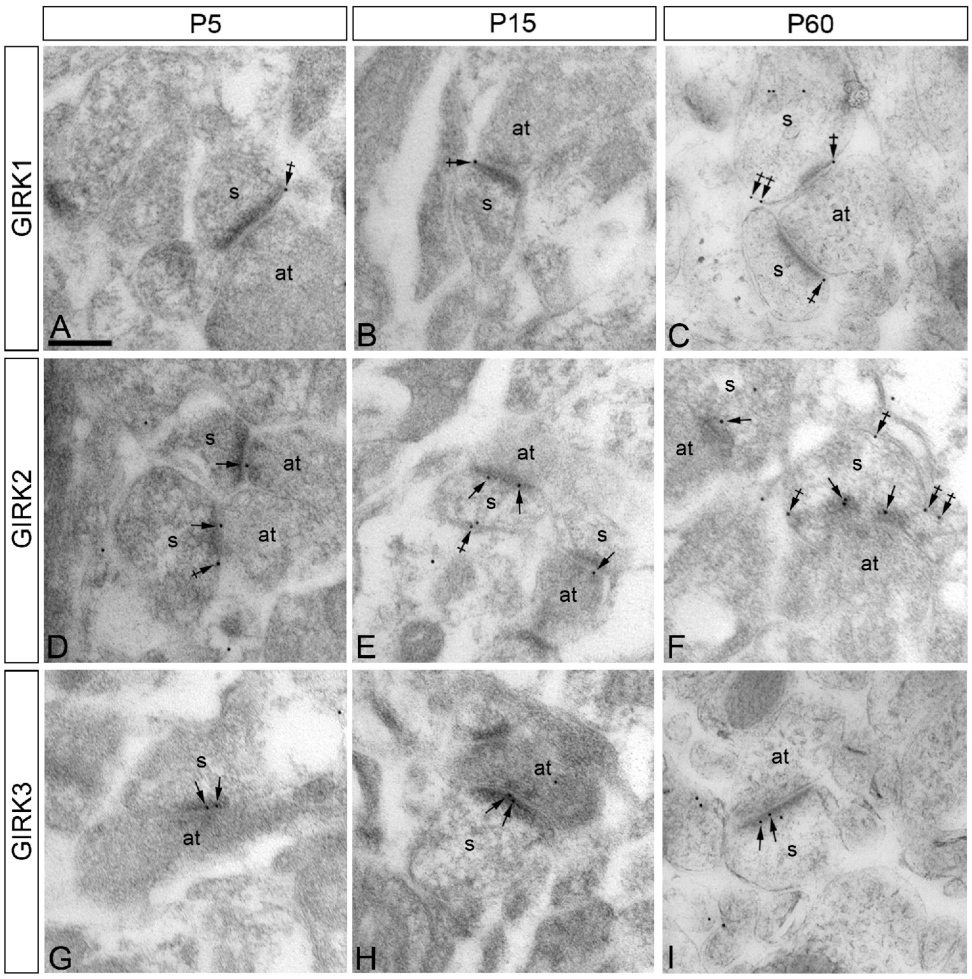

Fig. 7.

Electron micrographs of the CA1 region of the hippocampus showing immunoparticles for GIRK1, GIRK2 and GIRK3 in the *stratum radiatum*, as detected using a postembedding immunogold method at P5, P15 and P60. (A-C) GIRK1 was never detected along the PSD of dendritic spines (s) of CA1 pyramidal cells establishing asymmetrical synapses with axon terminals (at), probably Schaffer collaterals, at any developmental age. Immunoparticles for GIRK1 were only found at extrasynaptic or perisynaptic sites (crossed arrows). (D-F) Immunoreactivity for GIRK2 at the PSD (arrows) was low at P5, increased at P15 and was high at P60. Immunoparticles for GIRK2 were also detected at extrasynaptic or perisynaptic sites (crossed arrows). (G-I) Immunoreactivity for GIRK3 at the PSD (arrows) was similar throughout postnatal development. Scale bar: 0.2 μm.

Table 1

Summary of immunoparticle density for GIRK1, GIRK2 and GIRK3 in different subcellular compartments at P60

	GIRK1	GIRK2	GIRK3
Subcellular compartment	**Density (immunoparticles/μm²)**	**Density (immunoparticles/μm²)**	**Density (immunoparticles/μm²)**
Spines (SLM)	9.1 ± 0.6	9.6 ± 0.6	3.5 ± 0.4#
Spines (SR, distal)	8.6 ± 0.4	8.8 ± 0.5	3.1 ± 0.4#
Spines (SR, proximal)	5.3 ± 0.4*	5.7 ± 0.3*	3.2 ± 0.4#

* P <0.001 for proximal SR compared with distal SR and SLM.

# P <0.001 for GIRK3 density compared with GIRK1 and GIRK2.

Table 2

Summary of immunogold labelling for synaptic GIRK channel subunits during postnatal development

		P5	P15	P60
GIRK1	No. of immunoparticles	0	0	0
	No. of synapses	85	91	96
	Synapses labelled (%)	0	0	0
	Immunoparticles/labelled synapse	0	0	0
GIRK2	No. of immunoparticles	31	59	118
	No. of synapses	87	85	92
	Synapses labelled (%)	34	38	51
	Immunoparticles/labelled synapse[#]	1.03± 0.1	1.84 ± 0.1	2.51 ± 0.1
GIRK3	No. of immunoparticles	44	52	71
	No. of synapses	82	84	93
	Synapses labelled (%)	38	40	49
	Immunoparticles/labelled synapse	1.47 ±0.1	1.53 ± 0.1	1.54 ± 0.1

[#]Three-way comparison shows each age to be significantly different from every other age.